Carbon Trends 5 (2021) 100095

Contents lists available at ScienceDirect

Carbon Trends

journal homepage: www.elsevier.com/locate/cartre

# Enhanced heterogeneous electron transfer kinetics in Graphene Oxide produced from mechanically milled Graphite

R. Ashwini[a,b], Zinia Mohanta[c], M.K. Punith Kumar[d], Mysore Sridhar Santosh[a], Chandan Srivastava[d,*]

[a] Centre for Incubation, Innovation, Research and Consultancy (CIIRC), Jyothy Institute of Technology, Tataguni, Off Kanakapura Road, Bengaluru 560082, Karnataka, India
[b] Visvesvaraya Technological University, Jnana Sangama, Machhe, Belgaum 590018, Karnataka, India
[c] Center for Biosystems Science and Engineering (BSSE), Indian Institute of Science, C.V. Raman Road, Bengaluru 560012, Karnataka, India
[d] Department of Materials Engineering, Indian Institute of Science, C.V. Raman Road, Bengaluru 560012, Karnataka, India

ARTICLE INFO

*Article history:*
Received 21 June 2021
Revised 28 July 2021
Accepted 9 August 2021

*Keywords:*
Ball milling
defects
graphene oxide
$sp^3/sp^2$ hybridization
heterogenous electron transfer (HET) kinetics

ABSTRACT

Controlled structural and chemical defects were induced on to graphene oxide (GO) by mechanical milling of the precursor graphitic sheets for different times followed by their chemical oxidation. Raman, XRD, FTIR, XPS and AFM measurements was carried out as an evidence to study the structural and chemical modifications. Milling induces in plane and edge plane defects on graphitic sheets which influence oxidation degree, $sp^3/sp^2$ hybridization and functional groups constitution on produced GO. The influence of these structural variations towards electrochemical heterogenous electron transfer (HET) kinetics was explored using redox probe potassium ferricyanide and through non-enzymatic electrochemical detection of Hydrogen Peroxide ($H_2O_2$). The increased in-plane and edge plane functionalities actively enhanced the HET kinetics on GO and therefore it's the sensing ability significantly.



## 1. Introduction

The sensing ability of an electrode material greatly depends on the heterogenous electron transfer (HET) kinetics and surface interaction with the analyte [1, 2]. Carbon allotropes like graphene, graphene oxide (GO) and CNTs are well-known for their electrocatalytic activities, particularly in biosensing applications [3-5]. These carbon allotropes are also used to modify the electrodes in order to enhance their electrochemical performance, especially in the sensing of glucose, amino acids, proteins and other biomolecules [6-10]. Oxygenated functional groups present on GO aid in the anchoring of catalytic materials or metal oxide nanoparticles with a high specific surface area, making the nanoparticle decorated GO an ideal material for the construction of electrochemical sensors [11, 12]. Graphene oxide-based composites whose properties are superior compared to individual components are explored for non-enzymatic electrochemical detection of biomolecules [13]. GO-nanoparticle based composites such as, PtNi nanoparticles decorated rGO [14], GO-silica nanoparticle composite [15] and chemically reduced GO (rGO) [16] etc., are widely employed for the non-enzymatic detection of $H_2O_2$ and other biomolecules as well. However, the production of these composite materials involves multiple steps and the chemical reduction of GO to rGO requires a treatment with reducing agents such as hydrazine hydrate, tannic acid, etc. which are harsh and toxic [17].

Typically, the as-synthesized GO is used as the precursor to produce reduced graphene oxide (rGO) or graphene-based composites, but pristine GO itself is not preferred much for electrocatalytic applications due to its insulating nature. Recent studies, however, have shown that GO outperforms rGO and graphene as an electrocatalyst towards the redox probes and this is attributed to the presence of edge plane sites and oxygenated functional groups in GO [18], which act as heterogenous catalytic sites for electrochemical reactions [18-21]. GO modified with carboxyl functional (COOH) groups can mimic the horseradish peroxidase (HRP) enzyme activity in the detection of hydrogen peroxide ($H_2O_2$) [22, 23]. This illustrates that oxygenated or functionalized GO sheet can effectively work as electrode materials for non-enzymatic detection of biomolecules. The enhanced electrochemical behaviour of such GO modified electrodes are quantified based on the HET kinetics near the surface of the electrode [24]. The insight from the previous studies reveal that the edge plane sites/defects predominates HET

* Corresponding Authors: Dr. Chandan Srivastava Materials Engineering, IISC Bangalore: Indian Institute of Science, India
*E-mail address:* csrivastava@iisc.ac.in (C. Srivastava).

https://doi.org/10.1016/j.cartre.2021.100095

rate when compared to contribution from the basal plane sites [25, 26]. Interestingly, structural contributions in enhancing the electrochemical behaviour of GO sheets was investigated by inducing edge plane defects or varied degree of oxidation either through sonication or chemical reduction of GO sheets [27, 28].

In this study, the edge plane and in-plane defects were initially induced on graphitic sheets by mechanical milling for different times and these graphitic sheets were then chemically exfoliated to produce a series of GO samples with different degree of oxidation. Mechanical milling process damages the graphitic planes leading to the creation of a large number of structural defects such as edge plane defect, vacancies and interplane $sp^3$ bonds [29-31]. Upon chemical oxidation, these defect sites are the preferred ones for the anchoring of the oxygen-containing functional groups such as carboxyl, carbonyl and hydroxyl groups in the GO structure. Hence, the creation of structural defects on the graphitic precursors before their oxidation will increase the defects and the oxygen moieties in the produced GO structure [32-34]. As synthesized, milling modified GO was used to study the influence with HET rate on modified electrodes for electrocatalytic applications.

In the present work, graphite powder was ball milled for different hours e.g., 10 h, 20 h and 50 h prior to the chemical oxidation process. The resultant respective GO samples were named as GO-0 h, GO-10 h, GO-20 h and GO-50 h (hours represent milling time of the precursor used to prepare GO). The as-produced GO samples showed a variation in aromatic to non-aromatic carbon content ($sp^3/sp^2$ ratio), functional group constitution and defects. The effect of these parameters on the electrochemical behaviour was investigated using the electrochemical redox probe potassium ferricyanide [$K_3Fe(CN)_6$] and also towards the enzyme less detection ability for hydrogen peroxide ($H_2O_2$).

## 2. Materials and methods

**Materials:** Graphite powder with 99.99% purity (100 microns, SDFCL, India) were used as precursors for the synthesis of graphene oxide (GO). 30% (w/v) hydrogen peroxide ($H_2O_2$) was used after diluting it in 0.1M phosphate buffer solution (PBS). All other chemicals and solvents purchased were of AR grade from SDFCL, India, and were used without further purification, unless specified otherwise.

### 2.1. Synthesis of graphene oxide (GO)

A two-step process was followed for the synthesis of graphene oxide as reported elsewhere [33]. In brief, milling of graphite powder was carried out at different time intervals (10 h, 20 h and 50 h). High purity graphite powder of equal weight was transferred into a two hard chromium steel vials containing stainless steel balls. The ball to powder ratio was maintained to be 1:25. 100 mL of Hexane was added to each of the bowls and were sealed using Teflon. The specifications of the set program to carry out milling cycles at different time intervals was, bowl speed - 300 rpm, plate speed – 720 rpm, ON time – 10 minutes and OFF time – 08 minutes between each cycle to avoid excessive heating of the machine.

Following this, the milled graphite powder was used as a precursor for the synthesis of GO using Tour's method [35]. A mixture of graphite and potassium permanganate ($KMnO_4$) in the ratio of 1:6 (w/w) was taken in a beaker into which solution of sulfuric acid and orthophosphoric acid (9:1 v/v) was added while keeping the beakers in ice bath. The above mixture was stirred continuously for 12 hours at 45$^o$C. Then, the mixture was slowly transferred into a beaker containing 140 mL of distilled water ice, further to the same solution 10 mL of $H_2O_2$ was added. The final yellow colored mixture was washed several times using DI water and ethanol. The mixture was dried to obtain series of GO powder respective of milling time.

Hereafter, the milled graphitic precursors at different time intervals (10h, 20h, 50h) are referred as MG -10 h, MG -20 h and MG -50 h respectively. Un-milled graphitic precursor used to produce GO - 0 h is referred as graphite itself. GO samples are referred as GO- 0 h, GO-10 h, GO-20 h, GO-50 h, where 10, 20 and 50 indicate the milling times of graphite powder and GO – 0 h being the GO produced from un-milled graphite.

### 2.2. Graphene oxide characterization

The as-prepared GO samples and the milled graphitic precursors at different time intervals (10 h, 20 h and 50 h) were characterized using Raman (LabRam HR with 532nm laser), X-ray diffraction (XRD: JEOL Xpert Pro, PAN analytical JDX-8030 diffractometer Cu K-alpha X-ray source) and Fourier Transform Infrared Spectroscopy (FTIR: Perkin Elmer Frontier FT-NIR/MIR spectrometer). Dry powder samples were used for the measurements. X-ray Photoelectron Spectroscopy (XPS) elemental analysis (Kratos XPS Ultra Spectroscope, Al-K-$\alpha$ x-ray source) was carried out to obtain the relative content of aromatic and non-aromatic carbon content in the GO samples. GO samples were drop casted on 5 X 5 mm Si wafers for XPS analysis. Atomic force microscopic (AFM) images of GO samples were recorded using NX – 10 AFM instrument (Park system) in non-contact mode. The GO samples were drop dried on silicon wafers. An Al back coated Si Probe (ACTA, App Nano Inc, USA) with resonant frequency of 300 kHz having a nominal spring constant of 40 $Nm^{-1}$ was used. The images of 2 µm X 2 µm was acquired at a scan rate of 0.8 Hz. Finally, the images were processed using the XEI software.

### 2.3. Preparation of GO modified glassy carbon electrode (GCE) as working electrode

GCE was initially polished with alumina slurry and sonicated in ethanol for a few seconds to remove unwanted residues and contaminations. 1 mg of the as-synthesized graphene oxide (GO) samples was dispersed in 1 mL of water through sonication to give a homogenous suspension. Suspensions of 4 different samples GO-0h, GO-10h, GO-20h and GO-50h were prepared. 5$\mu$L of the suspension was then drop casted on cleaned GCE and then, the electrode was dried at room temperature. Thus, the GCE-GO-0h, GCE-GO-10h, GCE-GO-20h and GCE-GO-50h were obtained as modified working electrodes.

### 2.4. Electrochemical characterization

Cyclic voltammetry (CV) and chronoamperometry experiments were carried out using a CHI604E (CH Instruments, USA). A conventional 3 electrode cell containing a freshly prepared 2 mM $K_3Fe(CN)_6$ in 0.1M KCl and 0.1 M PBS of pH 7.4 was used as supporting electrolytes for the electrochemical measurements. GCE of 3 mm diameter modified with as-synthesized GO samples was used as the working electrode against a saturated Ag/AgCl (1M KCl) as reference and platinum wire as counter electrode for all the experiments.

Initially, cyclic voltammetry (CV) measurements were carried for 2 mM $K_3Fe(CN)_6$ in 0.1M KCl for different GO series in order to determine peak-to-peak separation potentials ($\Delta E_p$), electrochemical active surface area ($A_{eff}$), heterogenous electron transfer (HET) rate constant [$k^0$], peak currents [$I_p$] and sensitivity parameters.

CV measurements were also carried out at optimized potential ranges from 0 V to -1.4 V for the reduction of $H_2O_2$ using 0.1 M PBS at pH 7.4. $H_2O_2$ detection was carried out at different scan rates from 10 mV/s to 50 mV/s for the concentrations 2

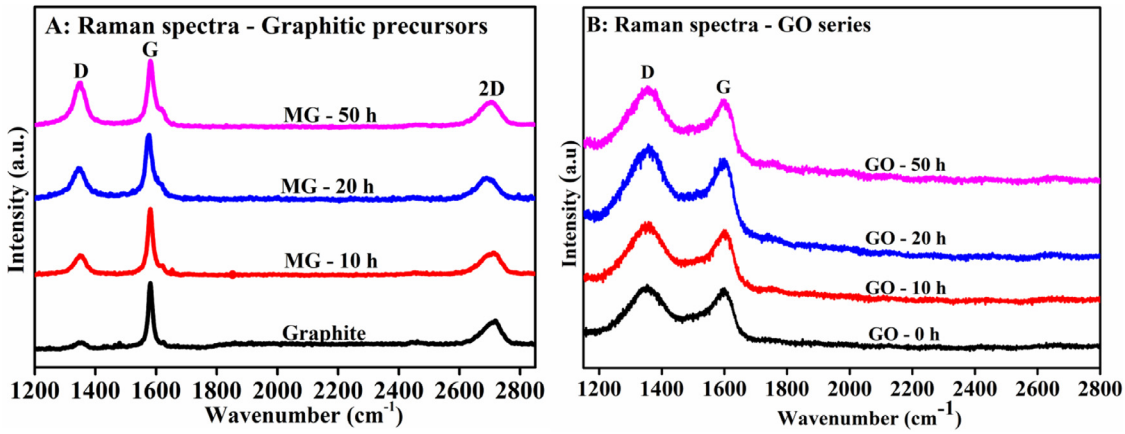


**Fig 1.** Raman spectra for (A) milled graphitic precursors at different time interval (B) Graphene oxide produced from milled graphitic precursors.

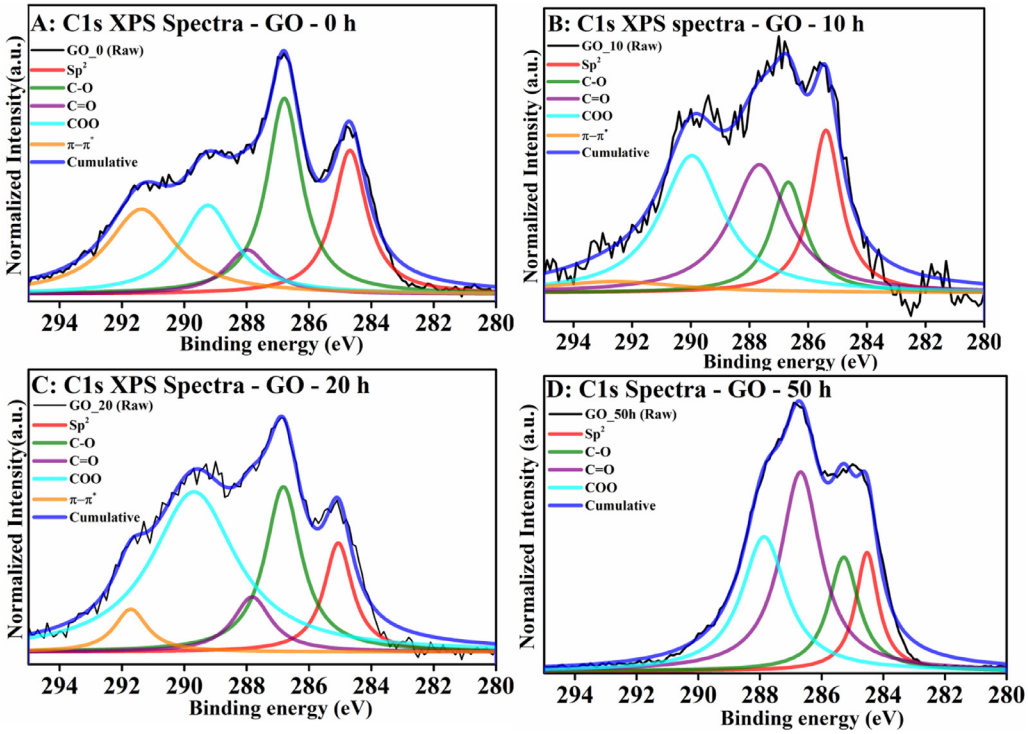


**Fig 2.** XPS spectra for GO series - A: GO-0 h, B: GO-10 h, C: GO-20 h, D: GO-50 h.

mM to 10 mM (2,4,6,8 and 10) in 0.1 M PBS. The electrochemical measurements were carried out for all the samples of GO as mentioned above and the results were compared with GO produced from un-milled graphite (GO-0h). Chronoamperometry responses were recorded at the applied potential of -0.6 V for GO-0h and at -0.4 V for GO-10h, GO-20h and GO-50h respectively for 10 minutes with the addition of 0.5 mM $H_2O_2$ at every 60 seconds. All the experiments were carried out at room temperature in triplicates.

## 3. Results and discussion

### 3.1. Raman spectroscopy

Raman spectra of the milled graphitic samples is given in Fig.1(A). D and G band in the Raman spectra denotes the presence of $sp^3$ and $sp^2$ hybridized carbon atoms respectively. The increase in the D band intensity indicates an increase in $sp^3$ hybridized carbon bonds or defects in the structure [36]. In addition, the spectrum points out the formation of $sp^3$ bonds in the graphitic structure due to the milling process. The intensity ratio of the D band to G band ($I_D/I_G$) indicates structural defects [36]. From Fig.1(A), $I_D/I_G$ ratio for the milled graphitic precursors – MG - 0h, 10 h, 20 h and MG 50h were 0.53, 0.71, 0.85 and 1.01 respectively, indicating the increasing order of defects as MG-0 h<MG-10 h< MG-20 h< MG-50 h.

Raman spectra for the GO series is shown in Fig.1(B). Increase in the D band intensity can be observed in the GO samples from GO-0 h to GO-50 h. From the Fig.1(B), $I_D/I_G$ for GO-0 h to GO – 50 h were 1.04, 1.08, 1.09, 1.10 respectively, indicating increase in $sp^3$ hybridized carbon atoms from GO – 0 h to GO – 50h. The defects in the GO samples increases in the order GO-0 h< GO–10 h< GO–20 h<GO–50 h, where the extent of defects formation in GO followed the trend observed in the milled graphitic precursors, suggesting preferred oxidation at the defect sites [33].

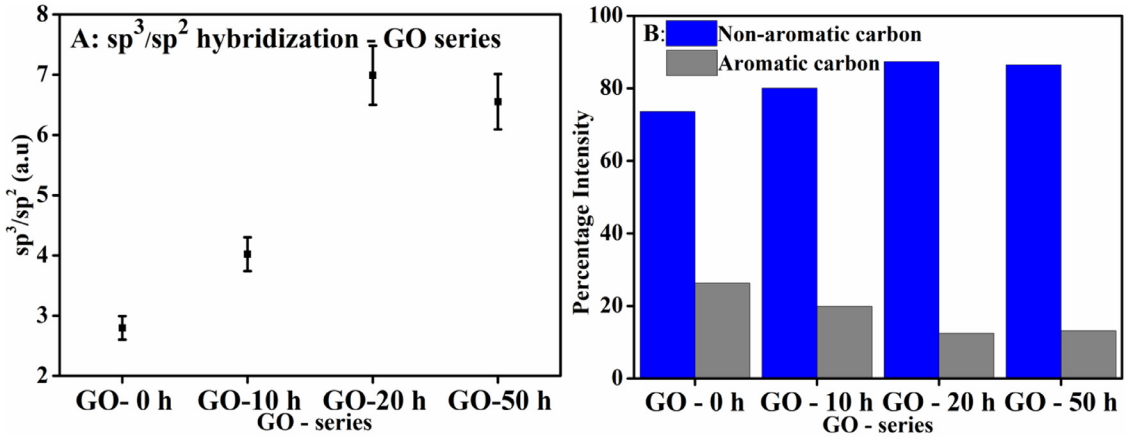


**Fig 3.** (A) Variation in the $sp^3/sp^2$ hybridization among the GO series; **(B)** Representing relative intenstites of aromatic and non-aromatic carbon content through the GO series.

### 3.2. X-ray diffraction studies

Figure S1(A) represents the characteristic XRD patterns showing (002) peak for pristine and milled graphitic precursors at different time intervals respectively. Figure S1(B) depicts XRD patterns showing the (001) peak for the GO series. The interlayer/d-spacing values between graphitic precursors and GO sheets were calculated using the Bragg's Law: $d = \lambda_0/2sin\theta$. The d-spacing values for the graphitic precursors - graphite, MG-10h, MG-20h and MG-50h were found to be equal to 3.36, 3.37, 3.36 and 3.39 Å respectively. Similarly, d-spacing values for GO series – GO-0h, GO-10h, GO-20h and GO-50h were found to be equal to 9.3, 9.43, 9.55, 9.78 Å respectively. By virtue of the increase in oxygen containing moieties, an increase in the interlayer spacing was observed along the GO series. This represents an increase in the level of oxidation which can be attributed to the oxidation at the site of defects created upon milling graphitic precursors [33]. The results of FTIR and AFM measurements are discussed in supplementary information.

### 3.3. X-ray photoelectron spectroscopy studies

Generally, the catalytic reactions occur at the heterogeneous catalytic surfaces. The oxygenated functional groups, $sp^3/sp^2$ ratio of the hybridized carbon content in the GO structure determine the catalytic behaviour of the GO sample [29, 31, 34]. The XPS spectra in Fig:2 reveals the presence of oxygen containing functional groups and C-C ($sp^2$) type bond hybridization among the GO samples.

Deconvolution of high-resolution C1s XPS spectra was carried out for the five groups: COO- at ~290.3 eV, C=O at ~287.9 eV, C-O at ~286.7 eV, $sp^2$ at ~285 eV and ~292 eV respectively. An increase in the percentage of oxygen- containing functional groups along the GO series (increasing milling time) were observed to suggest different degree of oxidation [33]. The aromatic to non-aromatic carbon content ($sp^3/sp^2$) ratio was determined using the formula:

$$\frac{sp^3}{sp_2} = \frac{(\%\ intensity\ of\ non-aromatic\ carbon\ content)}{(\%\ intensity\ of\ aromatic\ carbon)} \quad \text{(Equation - 1)}$$

From Fig: 3A, the $sp^3/sp^2$ ratio was found to increase linearly along the GO series indicating an increase in the $sp^3$ hybridized carbon domains which was in agreement with the effect of graphitic precursor milling duration. From Fig: 3B, the linear increase in the non-aromatic carbon content can be clearly observed indicating the accumulation of more oxygen functional groups. During the initial milling hours, due to breakage of graphitic sheets, edge plane defects were created leading to more edge plane carboxyl groups (COO) [33, 37, 38]. Whereas at higher milling hours, the sintering of graphitic sheets caused a higher percentage of in-plane defects leading to the presence of carbonyl and hydroxyl functional groups at a higher percentage on the produced GO sheets [33, 37, 38]. The $\pi \rightarrow \pi^*$ interaction is a characteristic feature of aromatic compounds and the $\pi \rightarrow \pi^*$ interaction is comparatively lesser in GO since GO is a nonaromatic surface containing $sp^3$ hybridized carbon atoms with isolated $sp^2$ carbon domains. Hence, the suppression of $\pi \rightarrow \pi^*$ satellite peak in XPS spectra at ~292 eV among GO series reveals the increased $sp^3$ carbon atoms [39].

The Raman and XPS analyses indicate that the structural variations on GO sheets can be created by ball milling the graphitic precursors used to synthesize GO that may influences the heterogeneous catalytic surface on the GO sheets [31, 32]. The AFM images are provided in fig: S2 from which, the average sheet thickness of the GO sheets was determined using the line profiles. The $I_D/I_G$ ratio, oxidation degree and the average thickness of the sheets among the GO series calculated from the above analysis are given in table 1.

### 3.4. Electrochemical characterization

The electrocatalytic nature of the GO series was investigated for the redox probe $K_3Fe(CN)_6$ and for the detection of $H_2O_2$ via cyclic voltammetry (CV) measurements. The influence of structural variations through enhanced functionalities and edge plane sites on the catalytic behaviour of GO samples was evaluated by peak-to-peak separation potentials [$\Delta Ep$], electrochemical active surface area [$A_{eff}$], HET rate constant [$k^0$], peak currents [Ip] and sensitivity parameters.

Fig: 4A - represents the cyclic voltammograms of GO series for the probe $K_3Fe(CN)_6$ at different scan rates. The nature of voltammogram for the GO samples (GO – 10 h, 20 h and 50 h) produced from milled graphite appears to be different compared GO-0 h. The peak separation potential ($\Delta E_P$) and peak current (Ip) increases linearly with respect to the scan rate for GO-0 h (A1) and GO-10 h (A2), whereas for the samples GO-20 h (A3) and GO-50 h (A4) - $\Delta Ep$ remains approximately constant with a linear increase in the peak currents.

Further, the $\Delta Ep$ values among the GO series were calculated from the Fig. 4 - A5, and is in the order GO-0 h > GO-10 h > GO-20 h > GO-50 h. A decrease in the $\Delta Ep$ indicates towards the presence of more heterogenous catalytic surface. This can be attributed to the enhanced edge plane defects, functionalities on the

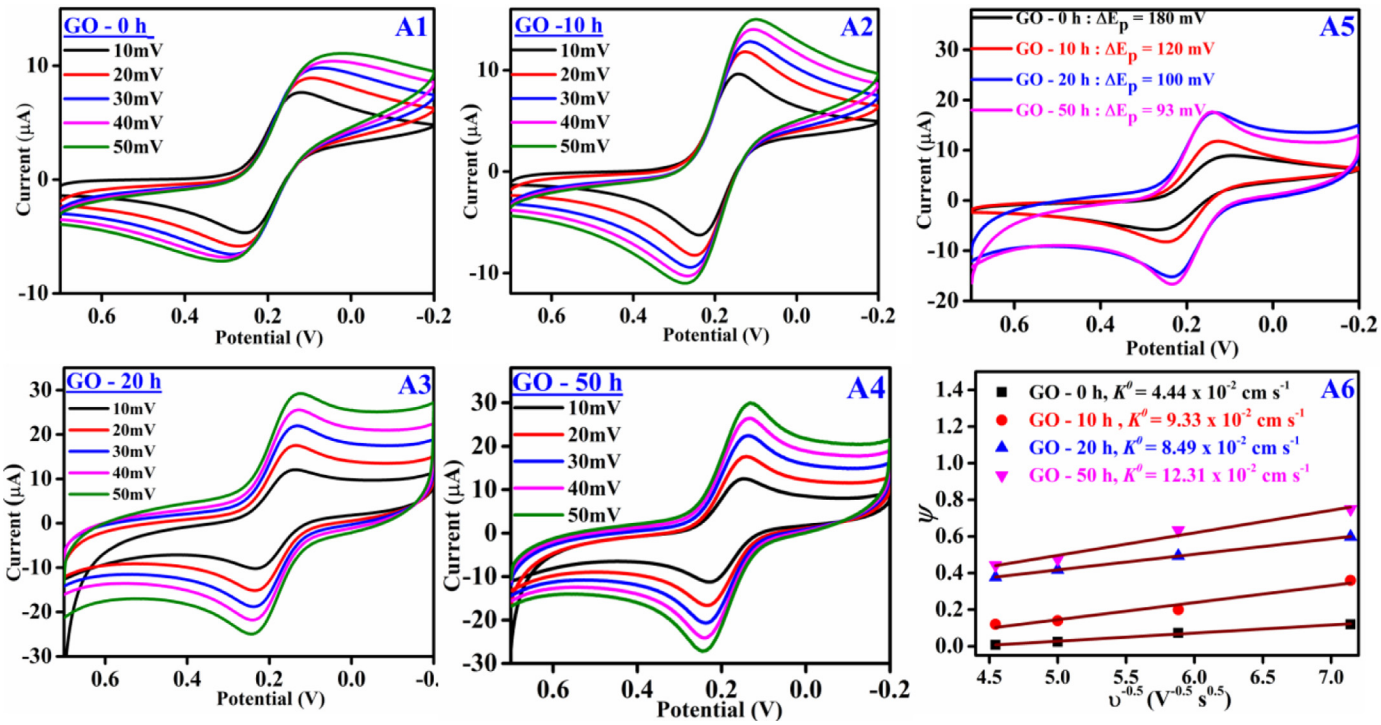


**Fig 4.** Cyclic voltammogram of GO series for the redox probe $K_3Fe(CN)_6$ and plot of HET constants - $k^0$.

**Table 1**
Representing structural variation parameters through GO series.

| GO series | $I_D/I_G$ | Oxidation degree | $sp^3/sp^2$ ratio | Average thickness of GO sheets (nm) |
|---|---|---|---|---|
| GO-0 h | 1.04 | 64.7 | 0.20 | 28.6 |
| GO-10 h | 1.08 | 80 | 0.28 | 26.1 |
| GO-20 h | 1.09 | 87.7 | 0.49 | 2.1 |
| GO-50 h | 1.1 | 86.8 | 0.46 | 3.1 |

electrode surface in the GO - 20 h and 50 h samples facilitating faster HET. This inference is supported by calculating the HET rate constant - $k^0$ . The $k^0$ for the electrochemical quasi-reversible process can be correlated with the diffusion rate, $\Delta Ep$ which increases with the scan rate and can be determined using the Nicolson analysis as mentioned in equation (2) [15]:

$$\psi = k^0\left(\frac{D_O}{D_R}\right)^{\alpha/2}\sqrt{\frac{RT}{\pi nF\upsilon D_O}} \qquad \text{(Equation – 2)}$$

Where $\psi$ is the dimensionless kinetic parameter determined from $\Delta Ep$, D is the diffusion coefficient of the electroactive species, n is the number of electrons transferred, F is the Faraday constant, $\upsilon$ is the applied scan rate, R and T have usual meanings. Equation 2 is valid for one step one electron process with $\Delta Ep < 220$ mV and diffusion coefficients considered to be approximately equal to the oxidation and reduction ($D_O$ *and* $D_R$) reactions, and $\alpha$ is the transfer coefficient equal to 0.5. Hence, equation (2) can be reduced to:

$$\psi = k^0\sqrt{\frac{RT}{\pi DF}}\ \upsilon^{-1/2} \qquad \text{(Equation - 3)}$$

In general, $\psi$ is calculated from $\Delta Ep$ and $k^0$ is determined from the slope of $\psi - \upsilon^{-1/2}$ corresponding to equation 3. The plot of $\Delta Ep$ obtained from CV against different scan rates for GO samples used to calculate $\psi$ is given in supplementary Fig.S4 and equation S1. The plot of forward peak currents versus square root of the scan rate ($\upsilon^{1/2}$) for individual GO samples is shown in Fig. S5, from which linear increase in the anodic currents indicates that the electrochemical process is diffusional controlled. The relation between kinetic parameter $\psi$ and inverse square root of the scan rate for the GO series is shown in Fig.A6. The linear gradient trend is followed for all the samples and the rate constant $k^0$ is calculated following equation (3). $k^0$ is observed to be increasing among the GO series, indicating a faster electron transfer. The electrochemical active surface area ($A_{eff}$) of the modified electrodes with GO samples was calculated using Randles-Sevcik equation 4 [26].

**Table 2**
Representing electrochemical parameters derived from CV measurements.

| GO Series | $\Delta Ep$ (mV) | $A_{eff}$($cm^2$) × $10^{-4}$ | $k^0$($cm\ s^{-1}$) ×$10^{-2}$ | Ip (slope) |
|---|---|---|---|---|
| GO-0 h | 180 | 0.188 | 4.44 | 0.86 |
| GO-10 h | 120 | 0.276 | 9.33 | 1.32 |
| GO-20 h | 100 | 0.968 | 8.49 | 4.42 |
| GO-50 h | 93 | 0.986 | 12.31 | 4.50 |

$$I_p = \left(2.65 \times 10^5\right)n^{3/2}D^{1/2}\upsilon^{1/2}CA_{eff} \qquad \text{(Equation – 4)}$$

Where $n$ = number of electrons transferred during the electrochemical process, $\upsilon$ = scan rate, $D$ = diffusion co-efficient of the redox process, C is the concentration of the redox probe, $A_{eff}$ is the electrochemical active surface area. The calculated parameters $\Delta Ep$, $k^0$, $A_{eff}$, slope derived from forward peak currents are provided in table 2. The trend followed in these parameters is evident, suggesting the effect of structural contribution in enhancing the HET.

Further, the electrochemical behaviour was evaluated based on enzyme less detection of $H_2O_2$ in 0.1 M PBS as a supporting electrolyte. The CV in Fig. 5 depicts the electrochemical reduction of

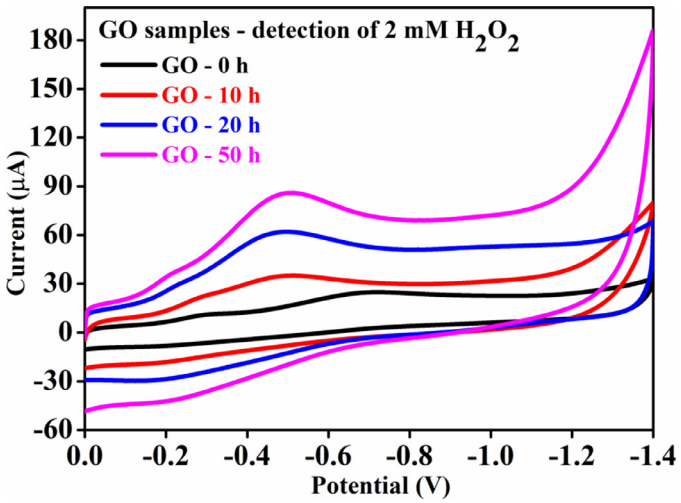


**Fig. 5.** Cyclic Voltammograms for GO in 2mM $H_2O_2$ at a scan rate of 40 mV/s.

2mM $H_2O_2$ on GCE modified electrode with different GO samples. The $H_2O_2$ reduction on GO - 0 h sample occurred at -0.6 V, whereas for the other GO samples, early reduction of $H_2O_2$ at -0.4 V with significant increase in the reduction current (GO-50 h> GO-20 h>GO-10 h>GO-0 h) was evident. The presence of varied oxygen functionalities among the GO series due to different degree of oxidation can contribute to the greater interaction of $H_2O_2$ on GO sheets. This facilitates a faster electron transfer that can reduce the working potential for the reduction of $H_2O_2$. Apparently, $COO^-$ in GO mimics the horseradish peroxidase enzyme in catalyzing $H_2O_2$ at a faster rate [22] and hence, an increase in the reduction current was noticed. In addition, the edge plane carboxyl functional groups lead to an early onset of reduction potential.

The effect of scan rate on the electrochemical response of GO samples in Fig.6 towards 2mM $H_2O_2$ reduction elucidates that the cathodic peak current as well as the peak potential increases linearly with a variation in the scan rate for all the samples. This ascertains the fact that $H_2O_2$ reduction on GO modified GCE electrode can be relatively slow and considerably limited by the scan rate. The inset figures in the cyclic voltammograms represent linear cathodic peak currents vs square root of the scan rates indicating that the electrochemical process is diffusion-controlled with the $R^2$ value between 96% to 98%.

Fig. 7(A–D) represent the electrochemical performance of GO modified GCE at varied concentrations of $H_2O_2$ from 2 mM to 10 mM at a scan rate of 40 mV/s. The cathodic reduction current linearly increases with an increase in the concentration of the analyte $H_2O_2$. In addition to the current, a significant linear shift in the cathodic reduction peak potential in the direction of sweeping potential was observed with an increase in the concentration of $H_2O_2$ for the samples GO-0h and GO-10h, wherein a minimal shift was observed for the samples GO-20h and GO-50h .

The linear dynamic range was observed for all the concentrations of $H_2O_2$ with respect to the reduction current as shown in Figure S7. The linear sensitivities corresponding to the slopes of the equations were 0.0062 μA/μM, 0.0075μA/μM, 0.018 μA/μM and 0.02 μA/μM, respectively (Fig. S7). The detection limit was calculated using the standard formula 3.3 X S.D./Slope, wherein 3.3 represents the background noise, S.D is the standard deviation obtained from the background current values without adding the analyte. Further, the sensitivity increases linearly with the GO series as mentioned in Table 3, whereas the increase in linearity was with respect to the milling time of the precursor graphite pow-

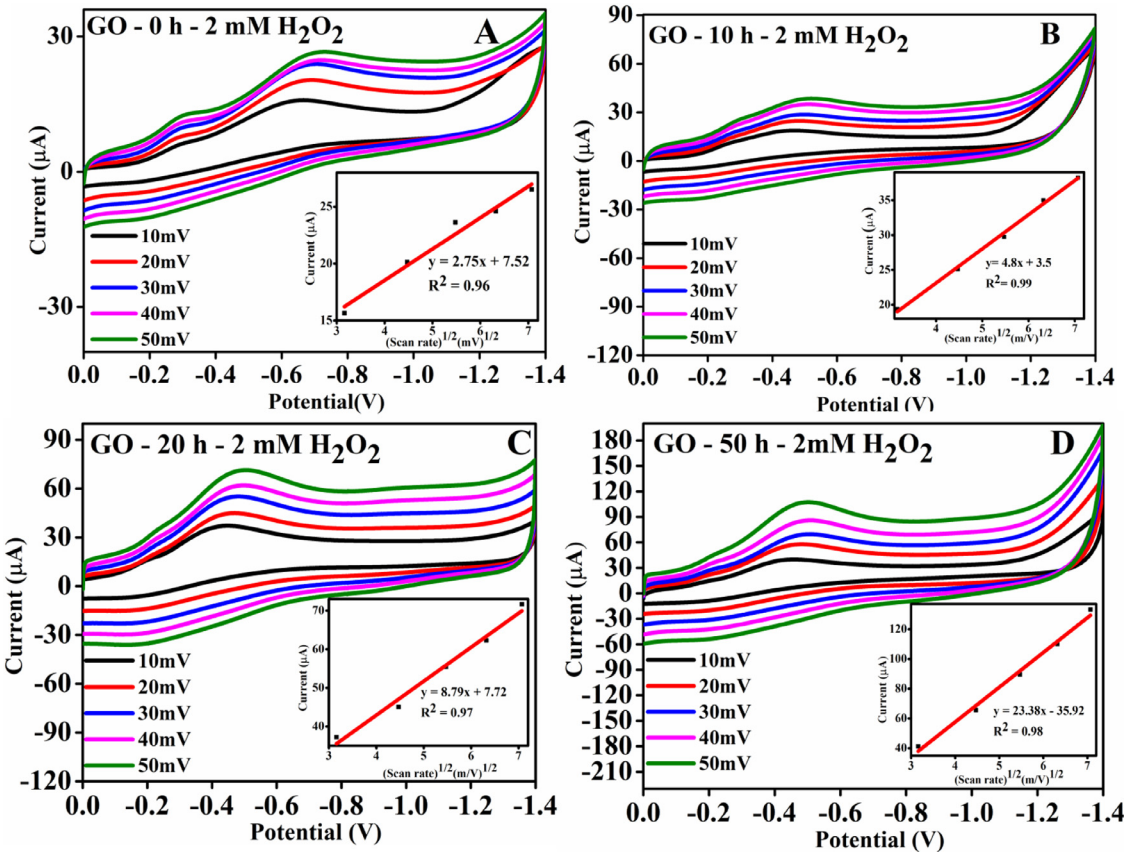


**Fig. 6.** The cyclic voltammograms from different GO samples for 2 mM $H_2O_2$ at different scan rates ranging from 10 mV/s to 50 mV/s.

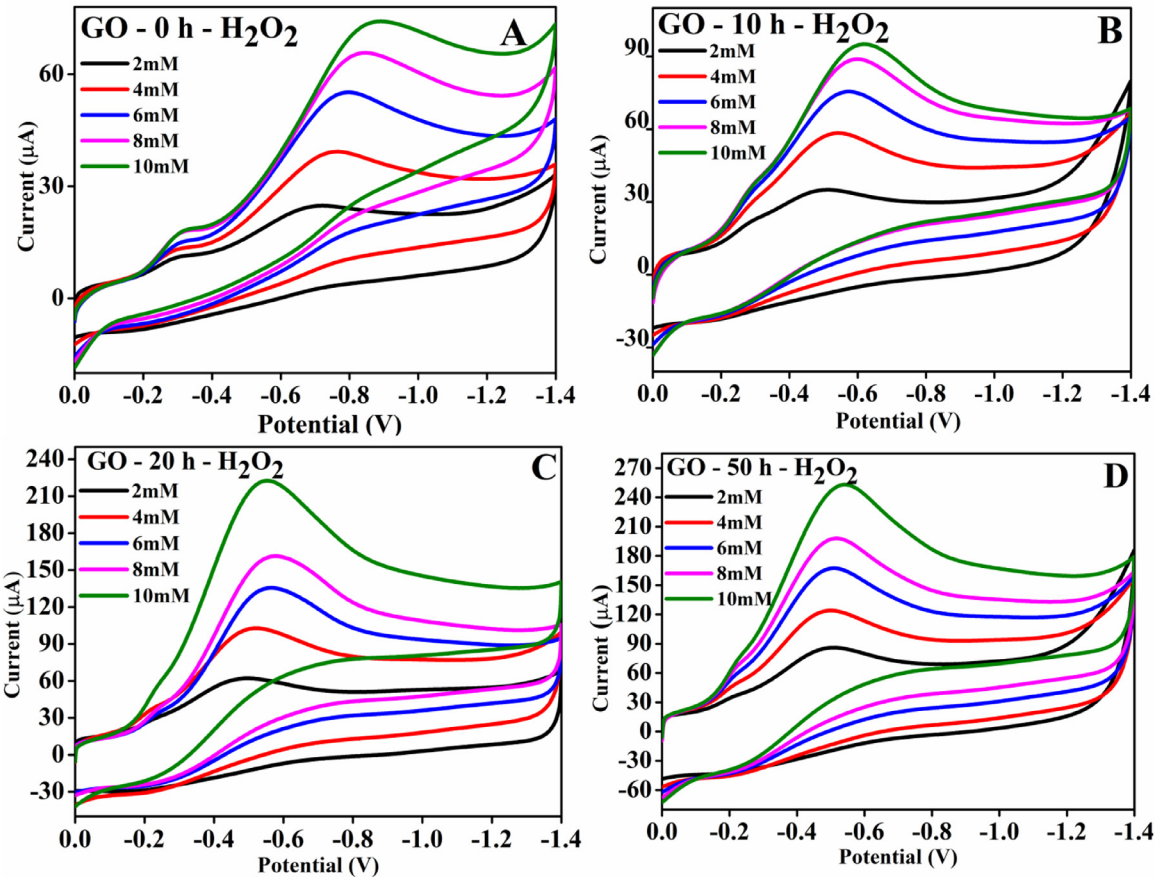


**Fig. 7.** Cyclic Voltammograms of GO samples with different concentrations of $H_2O_2$ ranging from 2 mM to 10 mM (2, 4, 6, 8 and 10 mM) at a fixed scan rate of 40 mV/s.

**Table 3**
Detection limit and linear sensitivities corresponding to the slopes of the equations.

| Electrode | Sensitivity (μA/μM) | Detection limit (μM) |
|---|---|---|
| GO-0 Hour | 0.0062 | 376.83 |
| GO-10 Hour | 0.0075 | 278.96 |
| GO-20 Hour | 0.018 | 152.30 |
| **GO-50 Hour** | **0.02** | **133.93** |

der that was used to produce graphene oxide and also the sensitivity among GO series can be correlated with the $sp^3/sp^2$ carbon content (Fig. 2), which is evident for the contribution of in-plane and edge plane functional groups. Sample GO-50 h showed an enhanced sensitivity with low detection limit compared to all other samples.

The chronoamperometry response on the addition of 0.5 mM $H_2O_2$ at approximately every 60 seconds has been shown in Fig. 8. The reduction of $H_2O_2$ for the sample GO-0 h was obtained at an applied potential of -0.6 V whereas, a reduction was obtained at -0.4 V for the samples GO-10 h, GO-20 h and GO-50 h. Already from the CV curves, we have observed the reduction potential has been shifted for the GO series obtained from milled graphite compared to GO-0h, and further, the same is represented from the chronoamperometry response (Fig. 8). Higher cathodic peak currents and improvement in the reduction potentials (-0.65 V to -0.4 V) can be attributed to better electrocatalytic effect among the GO series.

In general, the presence of structural defects/impurities and high edge plane to basal plane ratio among 2D materials results in the variation of density of states with unique electronic properties [13-15, 28] which in turn yields better electrochemical proper-

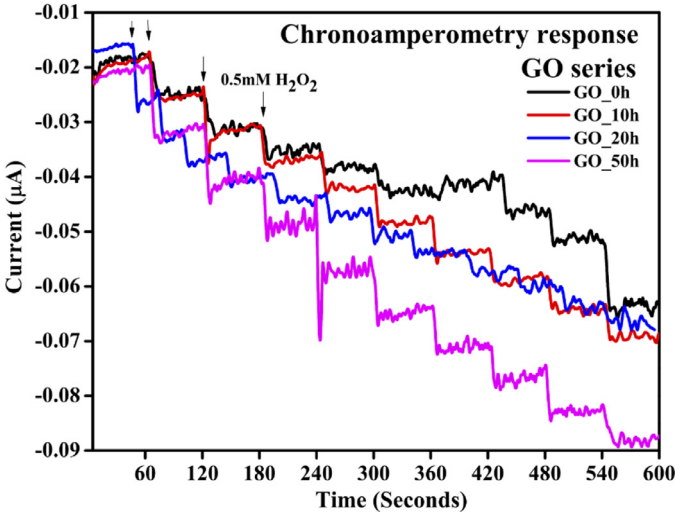


**Fig. 8.** Chronoamperometry response for GO series at applied potentials of -0.6 V for GO-0h and -0.4 V for GO-10h, 20h and 50h.

ties. Usually, such structural variations are achieved through techniques such as doping or producing rGO and GO based composites. In the present work, mechanical milling of graphitic precursors at different time intervals induced structural defects which led to evolution of oxygenated edge-plane and in-plane defects in the produced GO structures. As produced GO structures showed variations in the structural defects ($I_D/I_G$), oxidation degree and $sp^3/sp^2$ carbon content which can be correlated with the milling time of

the graphitic precursor. The influence of structural variations is evident in enhancing the electron transfer rates (HET) and for non-enzymatic detection of $H_2O_2$ at early onset working potential with higher sensitivity. Previous studies have shown GO enahnced with COOH groups [22] can mimic hydrogen peroxidase in detection of $H_2O_2$, however GO is subjected to chemical treatment in the process of producing GO-COOH. In the present work, as produced milled modified GO structures with enhanced functionlaities, without further chemical modification exhibit significant behaviour in detection of $H_2O_2$.

## 4. Conclusion

A feasible and green process has been reported in this study to control the degree of defect density in the GO to enhance its electrocatalytic activity. The mechanical milling of graphite induces defects into the graphitic planes and these pre-developed defects enhanced the oxidation at the GO edge and basal planes. The GO produced from milled graphite at different time intervals showed a better HET rate constant $k^0$, electrochemical active surface area, enhanced sensitivity and detection limit in the detection of $H_2O_2$ as compared to the GO from un-milled graphite. Among the GO produced from milled graphite (GO -10h, 20h and 50h), the linear increase in the $I_D/I_G$ and $sp^3/sp^2$ ratios as well HET kinetics - $k^0$ (Table 2 and 3) corelates with the increase in the milling time of the graphitic precursors. This indicates influence of structural defects and chemical functinalities in produced GO in enhancing electrochemical HET rates ($k^0$). GO-50h exhibited better results with respect to $k^0$, peak seperation potential, sensitivity and detection limits. Also, from the chronoamperometry response, an improvement in the reduction potential from -0.6 V (GO-0h) to -0.4 V (GO-10h, 20h, 50h) in the detection of $H_2O_2$ infers a betterment in the catalytic nature among the GO series. The enhanced electrochemical property of the milling modified GO, provides a suitable substitute for chemically reduced GO (rGO). This unique green approach used to ball-mill graphitic precursors in order to induce structural defects opens a new dimension to understand the surface phenomenon and encourages future researchers to develop applications based on such materials required for a multitude of applications.

## Declaration of Competing Interest

The authors declare that they have no known competing financial interests or personal relationships that could have appeared to influence the work reported in this paper.

## Acknowledgement

This work was supported by the KIRAN Division, Department of Science and Technology, Government of India under the Women Scientist Scheme-B (Project Grant No. DST/WOS-B/2018/2045/ETD/Ashwini). Funding from DST, Government of India is also gratefully acknowledged.

## Supplementary materials

Supplementary material associated with this article can be found, in the online version, at doi:10.1016/j.cartre.2021.100095.

## References

[1] V. Kumar, R.K. Gupta, R.K. Gundampati, D.K. Singh, S. Mohan, S.H. Hasan, M. Malviya, Enhanced electron transfer mediated detection of hydrogen peroxide using a silver nanoparticle-reduced graphene oxide-polyaniline fabricated electrochemical sensor, RSC Adv 8 (2018) 619–631, doi:10.1039/c7ra11466d.

[2] A. Ambrosi, C.K. Chua, A. Bonanni, M. Pumera, Electrochemistry of graphene and related materials, Chem. Rev. 114 (2014) 7150–7188, doi:10.1021/cr500023c.

[3] J.M. Goran, E.N.H. Phan, C.A. Favela, K.J. Stevenson, H2O2 Detection at Carbon Nanotubes and Nitrogen-Doped Carbon Nanotubes: Oxidation, Reduction, or Disproportionation? Anal. Chem. 87 (2015) 5989–5996, doi:10.1021/acs.analchem.5b00059.

[4] G. Gnana Kumar, K. Justice Babu, K.S. Nahm, Y.J. Hwang, A facile one-pot green synthesis of reduced graphene oxide and its composites for non-enzymatic hydrogen peroxide sensor applications, RSC Adv 4 (2014) 7944–7951, doi:10.1039/c3ra45596c.

[5] S.K. Krishnan, E. Singh, P. Singh, M. Meyyappan, H.S. Nalwa, A review on graphene-based nanocomposites for electrochemical and fluorescent biosensors, RSC Adv 9 (2019) 8778–8781, doi:10.1039/c8ra09577a.

[6] Z. Yang, C. Qi, X. Zheng, J. Zheng, Facile synthesis of silver nanoparticle-decorated graphene oxide nanocomposites and their application for electrochemical sensing, New J. Chem. 39 (2015) 9358–9362, doi:10.1039/c5nj01621e.

[7] W. Wen, Y. Song, X. Yan, C. Zhu, D. Du, S. Wang, A.M. Asiri, Y. Lin, Recent advances in emerging 2D nanomaterials for biosensing and bioimaging applications, Mater. Today 21 (2018) 164–177, doi:10.1016/j.mattod.2017.09.001.

[8] H. Wu, J. Wang, X. Kang, C. Wang, D. Wang, J. Liu, I.A. Aksay, Y. Lin, Glucose biosensor based on immobilization of glucose oxidase in platinum nanoparticles/graphene/chitosan nanocomposite film, Talanta 80 (2009) 403–406, doi:10.1016/j.talanta.2009.06.054.

[9] Y. Liu, D. Yu, C. Zeng, Z. Miao, L. Dai, Biocompatible graphene oxide-based glucose biosensors, Langmuir 26 (2010) 6158–6160, doi:10.1021/la100886x.

[10] H. Afsharan, B. Khalilzadeh, H. Tajalli, M. Mollabashi, F. Navaeipour, M.R. Rashidi, A sandwich type immunosensor for ultrasensitive electrochemical quantification of p53 protein based on gold nanoparticles/graphene oxide, Electrochim. Acta. 188 (2016) 153–164, doi:10.1016/j.electacta.2015.11.133.

[11] M. Thangamuthu, K.Y. Hsieh, P.V. Kumar, G.Y. Chen, Graphene- and graphene oxide-based nanocomposite platforms for electrochemical biosensing applications, Int. J. Mol. Sci. (2019) 20, doi:10.3390/ijms20122975.

[12] F. Xu, Y. Sun, Y. Zhang, Y. Shi, Z. Wen, Z. Li, Graphene-Pt nanocomposite for nonenzymatic detection of hydrogen peroxide with enhanced sensitivity, Electrochem. Commun. 13 (2011) 1131–1134, doi:10.1016/j.elecom.2011.07.017.

[13] S. Palanisamy, S.M. Chen, R. Sarawathi, A novel nonenzymatic hydrogen peroxide sensor based on reduced graphene oxide/ZnO composite modified electrode, Sensors Actuators, B Chem 166–167 (2012) 372–377, doi:10.1016/j.snb.2012.02.075.

[14] H. Gao, F. Xiao, C.B. Ching, H. Duan, One-step electrochemical synthesis of PtNi nanoparticle-graphene nanocomposites for nonenzymatic amperometric glucose detection, ACS Appl. Mater. Interfaces. 3 (2011) 3049–3057, doi:10.1021/am200563f.

[15] Y. Huang, S.F.Y. Li, Electrocatalytic performance of silica nanoparticles on graphene oxide sheets for hydrogen peroxide sensing, J. Electroanal. Chem. 690 (2013) 8–12, doi:10.1016/j.jelechem.2012.11.041.

[16] M. Zhou, Y. Zhai, S. Dong, Electrochemical sensing and biosensing platform based on chemically reduced graphene oxide, Anal. Chem. 81 (2009) 5603–5613, doi:10.1021/ac900136z.

[17] T. Liang, X. Guo, J. Wang, Y. Wei, D. Zhang, S. Kong, Green synthesis of porous graphene-like nanosheets for high-sensitivity nonenzymatic hydrogen peroxide biosensor, Mater. Lett. 254 (2019) 28–32, doi:10.1016/j.matlet.2019.06.100.

[18] D.A.C. Brownson, G.C. Smith, C.E. Banks, Graphene oxide electrochemistry: The electrochemistry of graphene oxide modified electrodes reveals coverage dependent beneficial electrocatalysis, R. Soc. Open Sci. 4 (2017), doi:10.1098/rsos.171128.

[19] D.A.C. Brownson, C.E. Banks, Graphene electrochemistry: Fabricating amperometric biosensors, Analyst. 136 (2011) 2084–2089, doi:10.1039/c0an00875c.

[20] D.A.C. Brownson, C.W. Foster, C.E. Banks, The electrochemical performance of graphene modified electrodes: An analytical perspective, Analyst 137 (2012) 1815–1823, doi:10.1039/c2an16279b.

[21] W.J. Lin, C.S. Liao, J.H. Jhang, Y.C. Tsai, Graphene modified basal and edge plane pyrolytic graphite electrodes for electrocatalytic oxidation of hydrogen peroxide and $\beta$-nicotinamide adenine dinucleotide, Electrochem. Commun. 11 (2009) 2153–2156, doi:10.1016/j.elecom.2009.09.018.

[22] Y. Song, K. Qu, C. Zhao, J. Ren, X. Qu, Graphene oxide: Intrinsic peroxidase catalytic activity and its application to glucose detection, Adv. Mater. 22 (2010) 2206–2210, doi:10.1002/adma.200903783.

[23] W. Sun, X. Ju, Y. Zhang, X. Sun, G. Li, Z. Sun, Application of carboxyl functionalized graphene oxide as mimetic peroxidase for sensitive voltammetric detection of H2O2 with 3,3′,5,5′-tetramethylbenzidine, Electrochem. Commun. 26 (2013) 113–116, doi:10.1016/j.elecom.2012.09.032.

[24] D.A.C. Brownson, A. Garcia-Miranda Ferrari, S. Ghosh, M. Kamruddin, J. Iniesta, C.E. Banks, Electrochemical properties of vertically aligned graphenes: tailoring heterogeneous electron transfer through manipulation of the carbon microstructure, Nanoscale Adv (2020) 5319–5328, doi:10.1039/d0na00587h.

[25] K.L.S. Castro, S.M. Oliveira, R.V. Curti, J.R. Araújo, L.M. Sassi, C.M. Almeida, E.H.M. Ferreira, B.S. Archanjo, M.F. Cabral, A. Kuznetsov, L.A. Sena, C.A. Achete, E. D'Elia, Electrochemical response of glassy carbon electrodes modified using graphene sheets of different sizes, Int. J. Electrochem. Sci. 13 (2018) 71–87, doi:10.20964/2018.01.02.

[26] A.J. Slate, D.A.C. Brownson, A.S. Abo Dena, G.C. Smith, K.A. Whitehead, C.E. Banks, Exploring the electrochemical performance of graphite and graphene paste electrodes composed of varying lateral flake sizes, 2018. https://doi.org/10.1039/c8cp02196a.

[27] P. Tan, Q. Bi, Y. Hu, Z. Fang, Y. Chen, J. Cheng, Effect of the degree of oxidation and defects of graphene oxide on adsorption of Cu 2+ from aqueous solution, Appl. Surf. Sci. 423 (2017) 1141–1151, doi:10.1016/j.apsusc.2017.06.304.
[28] K. Krishnamoorthy, M. Veerapandian, K. Yun, S.J. Kim, The chemical and structural analysis of graphene oxide with different degrees of oxidation, Carbon N. Y. 53 (2013) 38–49, doi:10.1016/j.carbon.2012.10.013.
[29] Y. Qiu, D. Fan, G. Lan, S. Wei, X. Hu, Y. Li, Generalized reactivity descriptor of defective carbon catalysts for acetylene hydrochlorination: The ratio of sp2 : sp3hybridization, Chem. Commun. 56 (2020) 14877–14880, doi:10.1039/d0cc06177h.
[30] D.W. Chang, H.J. Choi, I.Y. Jeon, J.M. Seo, L. Dai, J.B. Baek, Solvent-free mechanochemical reduction of graphene oxide, Carbon N. Y. 77 (2014) 501–507, doi:10.1016/j.carbon.2014.05.055.
[31] A.S. Milev, N.H. Tran, G.S.K. Kannangara, M.A. Wilson, Unoccupied electronic structure of ball-milled graphite, Phys. Chem. Chem. Phys. 12 (2010) 6685–6691, doi:10.1039/b926345d.
[32] D. Zhang, X. Zhang, X. Sun, H. Zhang, C. Wang, Y. Ma, High performance supercapacitor electrodes based on deoxygenated graphite oxide by ball milling, Electrochim. Acta. 109 (2013) 874–880, doi:10.1016/j.electacta.2013.07.184.
[33] Z. Mohanta, H.S. Atreya, C. Srivastava, Correlation between defect density in mechanically milled graphite and total oxygen content of graphene oxide produced from oxidizing the milled graphite, Sci. Rep. 8 (2018) 1–6, doi:10.1038/s41598-018-34109-z.
[34] A.E.D. Mahmoud, A. Stolle, M. Stelter, Sustainable Synthesis of High-Surface-Area Graphite Oxide via Dry Ball Milling, ACS Sustain. Chem. Eng. 6 (2018) 6358–6369, doi:10.1021/acssuschemeng.8b00147.
[35] D.C. Marcano, D.V. Kosynkin, J.M. Berlin, A. Sinitskii, Z. Sun, A. Slesarev, L.B. Alemany, W. Lu, J.M. Tour, Improved synthesis of graphene oxide, ACS Nano 4 (2010) 4806–4814, doi:10.1021/nn1006368.
[36] M.K. Punith Kumar, M. Nidhi, C. Srivastava, Electrochemical exfoliation of graphite to produce graphene using tetrasodium pyrophosphate, RSC Adv 5 (2015) 24846–24852, doi:10.1039/c5ra01304f.
[37] Z. Mohanta, S.K. Gaonkar, M. Kumar, J. Saini, V. Tiwari, C. Srivastava, H.S. Atreya, Influence of oxidation degree of graphene oxide on its nuclear relaxivity and contrast in MRI, ACS Omega 5 (2020) 22131–22139, doi:10.1021/acsomega.0c02220.
[38] A. Lerf, H. He, M. Forster, J. Klinowski, Structure of graphite oxide revisited, J. Phys. Chem. B. 102 (1998) 4477–4482, doi:10.1021/jp9731821.
[39] V. Georgakilas, J.N. Tiwari, K.C. Kemp, J.A. Perman, A.B. Bourlinos, K.S. Kim, R. Zboril, Noncovalent Functionalization of Graphene and Graphene Oxide for Energy Materials, Biosensing, Catalytic, and Biomedical Applications, Chem. Rev. 116 (2016) 5464–5519, doi:10.1021/acs.chemrev.5b00620.